TRENDS IN SCIENCES 2025; 22(7): 9971
https://doi.org/10.48048/tis.2025.9971
RESEARCH ARTICLE

Antifungal and Antibiofilm Activity of *Bacillus velezensis* BP1 Extract Against Candida *albicans*: *In Vitro* Bioassay, Metabolomics, *In Silico* Molecular Docking

Henra Henra[1,2], Ema Damayanti[3] and Jaka Widada[4,*]

[1]*Master Study Program of Biotechnology, Graduate School, Universitas Gadjah Mada, Yogyakarta 55281, Indonesia*
[2]*Doctoral Study Program of Agricultural Science, Agricultural Microbiology, Faculty of Agriculture, Universitas Gadjah Mada, Yogyakarta 55281, Indonesia*
[3]*Research Center for Food Processing and Technology, National Research and Innovation Agency (Badan Riset dan Inovasi Nasional), Gunungkidul 55861, Indonesia*
[4]*Department of Agricultural Microbiology, Faculty of Agriculture, Universitas Gadjah Mada, Yogyakarta 55281, Indonesia*

([*]Corresponding author's e-mail: jwidada@ugm.ac.id)

Received: 10 February 2025, Revised: 13 April 2025, Accepted: 20 April 2025, Published: 30 May 2025

Abstract

The biofilm-forming fungus *Candida albicans* is a leading cause of candidiasis disease, a condition complicated by the organism's notable resistance to antifungal treatments. While previous studies have identified various antifungal compounds produced by *Bacillus velezensis*, the antibiofilm efficacy of these compounds against *C. albicans* has not been thoroughly explored. This study presents a novel investigation into the secondary metabolites of *B. velezensis* BP1, focusing specifically on their dual action as antifungal agents and antibiofilm agents against *C. albicans*. Unlike earlier research that primarily examined the antifungal properties of *Bacillus* species in isolation, this study employs a comprehensive approach that integrates *in vitro* antifungal and antibiofilm activity assessments, metabolomic profiling, and *in silico* molecular docking analyses targeting proteins involved in biofilm formation. This multifaceted methodology allows for a deeper understanding of how BP1-P (biomass) and BP1-S (supernatant) extract from *B. velezensis* BP1 interact with *C. albicans*, revealing their capacity to inhibit biofilm formation through structural damage to the fungal hyphae (inhibition of proliferation) as concentrations increase (25 - 400 µg mL^{-1}). This research identifies 4 specific metabolites, betaine, oleamide, l-phenylalanine, and l-pyroglutamic acid that exhibit antifungal properties and demonstrate binding affinity to target proteins associated with biofilm development. The use of advanced imaging techniques such as scanning electron microscopy (SEM) and confocal laser scanning microscopy (CLSM) further distinguishes this study by providing visual confirmation of the morphological changes induced by treatment with BP1 extracts. Thus, BP1-P and BP1-S extract from *B. velezensis* BP1 can act as an effective antifungal and antibiofilm against *C. albicans*.

Keywords: *Candida albicans*, *Bacillus velezensis* BP1, Antifungal, Antibiofilm, Metabolomic profiling, Molecular docking

Introduction

Worldwide, 1.7 million people die from fungal infections every year, with immunocompromised people being the most affected [1,2]. The leading cause of candidiasis disease is the opportunistic fungus *Candida albicans* (*C. albicans*), responsible for human sickness [3]. Long-term antibiotic use can encourage the transformation of *C. albicans* into pathogenic cells (hyphae and pseudohyphae). Additionally, when the commensal environment and host defenses are out of balance, *C. albicans* can become an opportunistic fungus and spread disease [2,4]. Biofilm production as a structured community of fungal cells adhering to a

surface is a virulence factor determining *C. albicans* pathogenicity [4]. Biofilms can shield *C. albicans* from outside influences like antifungal medications, which can lead to numerous treatment failures and drug resistance [5]. The complexity of biofilm architecture allows *C. albicans* to evade both pharmacological treatments and host immune mechanisms, making infections difficult to manage [6,7].

Current antifungal therapies often fall short against biofilm-associated infections due to the protective nature of biofilms. The limited effectiveness of available treatments has led researchers to explore alternative strategies, including the use of natural products as potential antibiofilm agents [7,8]. Natural antimicrobial chemicals that produce bacteria can be converted into natural products [9]. Gram-positive *Bacillus* spp. are capable of secreting various bioactive compounds [10]. Generating secondary metabolites with antibiotic qualities is frequently linked to the antagonistic action of *Bacillus* species [11]. *Bacillus* species metabolite chemicals can cause intracellular damage, damage to the cell wall or membrane, and limit the growth of pathogenic fungi [7,12]. Secondary metabolite substances generated by *Bacillus* species that are antibiotic-active and can stop *C. albicans* from growing. These substances include lipopeptides (fengisin, surfactin, iturin), enzymes, polyketones, bacteriocins, and volatile compounds [7].

Supernatant (extracellular) and biomass (intracellular) metabolites in *Bacillus* are often compared to see the ability of cell components with products produced by bacteria to inhibit the growth of pathogenic microbes. Supernatant is a product produced and excreted by bacteria into the growth medium that contains various bioactive compounds. While biomass is a component of the bacterial cell itself, including enzymes, proteins, and metabolite compounds that accumulate in the cell [12,22]. Metabolomic data can be used to identify new therapeutic targets in candidiasis diseases [12,13]. Metabolomics is also important in biomarker identification and drug discovery [14]. Advanced secondary metabolite compound identification analysis can be done by molecular docking, a computational technique for analyzing the interaction between compounds and biofilm-coding proteins [15].

This study aimed to know the antifungal and antibiofilm activities BP1-P and BP1-S extract of *B. velezensis* BP1 isolates isolated from *Heterotrigona itama* nests. Continued research into metabolomics and molecular docking techniques may pave the way for novel therapeutic interventions that address the challenges posed by fungal infections. The metabolite compound analysis results will list new antifungal and antibiofilm agents from *B. velezensis* BP1 isolates against *C. albicans*.

Materials and methods

Bacterial strain and culture condition

B. velezensis BP1 isolate is a preparation owned by the BRIN Research Center for Food Technology and Processes (PRTPP). Cell-free culture supernatants were prepared by inoculating 10^6 cells mL^{-1} of *B. velezensis* BP1 in 60 mL of Tryptic Soy Broth (TSB) medium (Difco, Sparks, USA) and incubation at 28 °C for 24 h. After centrifugation at 4500×g for 10 min, the supernatant was kept at 4 °C until use. Strains classified as strong biofilm producers were included in the study as indicator strains for the antibiofilm assays, reference strains of the American Type Culture Collection (ATCC), *C. albicans* ATCC 10230. *C. albicans* isolates were streaked on Sabouraud dextrose agar (SDA) medium (Himedia AT180, Maharashtra, India) and then incubated for 24 h at 30 °C.

Metabolite extract production of *B. velezensis* BP1

The fermentation procedure for synthesizing secondary metabolites was conducted using the methods described [16,17] with slight adjustments. *B. velezensis* BP1 was cultivated at a temperature of 28 °C with an agitation rate of 180 rpm for 24 h. The cultivation was carried out in a 200 mL Erlenmeyer flask containing 60 mL of TSB medium (Difco, Sparks, USA). Subsequently, the cells were relocated into four 500 mL Erlenmeyer flasks, each holding 250 mL of TSB medium (Difco, Sparks, USA) for production. The flasks were then incubated for 5 days at a temperature of 28 °C, shaking at a speed of 180 rpm in a shaking incubator. The fermentation liquid was centrifuged at a speed of 4500×g for 10 min. This process separated the secondary metabolites in the biomass cells and cell-free

supernatants. The supernatant was extracted using ethyl acetate (1:1 v/v), and biomass cells were extracted with 200 mL of methanol. The liquid extract was subjected to evaporation to produce the crude extract. Supernatant extracts were encoded with BP1-S while extracts from cell biomass were encoded with BP1-P. After solvent evaporation, the extracts were stored at −20 °C until use.

Antifungal susceptibility test

The produced *B. velezensis* BP1 was assessed for its antifungal activity against *C. albicans* ATCC 10230 by measuring the minimum inhibitory concentrations (MIC_{50}) using 96-well microplates [18]. The microdilution methodology evaluated the antifungal activity with slight adjustments [4]. *C. albicans* colonies measuring approximately 1 mm in diameter were placed in sterile saline solution (0.85 % NaCl) and adjusted to a concentration of 0.5 McFarland standard (10^6 cells mL^{-1}). The suspension was then diluted at a ratio of 1:20 in Roswell Park Memorial Institute (RPMI) medium (Himedia AT180, Maharashtra, India) to achieve a concentration of approximately 10^3 cells mL^{-1}. A 100.000 µg mL^{-1} extract of *B. velezensis* BP1 metabolite was prepared by weighing 10 mg in a sterile Eppendorf tube. The extract was then diluted in 100 µL of 1 % dimethyl sulfoxide to create a stock solution. This stock solution prepared a 400 µg mL^{-1} extract concentration using RPMI 1640 medium. A total of 5 µL of *C. albicans* suspension was added to the wells of 96-well microplates containing 100 µL of double dilution in RPMI 1640 extract medium. Control treatments, namely media control, were also used in the assay. The assay was performed in triplicate. Incubation was carried out aerobically at 30 °C for 24 h. MIC determination was done to measure cell density at 540 nm (OD_{540}). MIC_{50} refers to the minimum inhibitory concentration effectively suppressing 50 % of the growth, as determined on a numerical scale [19].

Antibiofilm susceptibility test

Antibiofilm testing was conducted using the microdilution procedure [16] with slight adjustments, employing a colorimetric assay (MTT). *C. albicans* in RPMI 1640 media was cultivated in 96-well microplates and incubated without oxygen at 30 °C for 1.5 h for initial adhesion. The non-adherent cells (supernatant) were eliminated. A fresh RPMI 1640 medium was introduced into the microplate, with various extract concentrations ranging from 25 to 400 µg mL^{-1}. The control group, which contained no extract, was also included. The microplate was then incubated at 30 °C for 24 h. Subsequently, the biofilm was washed using a phosphate-buffered saline (PBS; pH 7.4) solution (Merck, Germany). A total of 100 µL of a solution containing 3-(4,5-dimethylthiazol-2-yl)-2,5-diphenyl tetrazolium bromide (MTT, Sigma-Aldrich) was introduced to the cleaned biofilm. The MTT reaction was incubated without light for 2 - 3 h at a temperature of 30 °C. 80 µL portion of the liquid was moved to a new 96-well microplate. The antibiofilm activity of the metabolite extract from *B. velezensis* BP1 was measured using a microplate reader at a wavelength of 490 nm (OD_{490}).

Biofilm quantification

Biofilm biomass was quantified with crystal violet (CV) staining (Merck, Germany). Cells not adhered to the biofilm after 24 h of incubation were eliminated by rinsing thrice with sterile PBS (Merck, Germany). The plates were dried, and cell fixation was carried out by adding 200 µL of 99 % methanol for 15 min. Subsequently, methanol was removed, and the drying process was carried out. Each well was treated with 200 µL of CV stain (1 %, v/v) and left to stain for 5 min. The residual CV was discarded, and the microplate was rinsed with sterile distilled water 3 times before being air-dried at room temperature. Each well was treated with 200 µL of acetic acid (Merck, Germany) solution (33 %, v/v) to remove the biofilm CV stain. A volume of 100 µL from the resultant solution was moved to a new microplate, and the absorbance was measured at a wavelength of 570 nm (OD_{570}). The experiment was carried out in triplicate, and the average absorbance of each well was plotted against the concentration of the extract. The fungal growth and biofilm formation percentages were determined using the following formula: (OD after treatment with extract) / (OD of control) × 100. Each well's average absorbance, fungal growth percentage, and biofilm formation percentage were graphed against extract concentration to analyze the data [16].

Scanning electron microscope (SEM) observation of *Candida albicans* biofilm cell damage

SEM observations were conducted by cultivating *C. albicans* biofilms on sterile acrylic (12 mm diameter) in a 24-well microplate at 30 °C for 48 h. The biofilms were grown with an inhibitory concentration of 100 µg mL^{-1} of *B. velezensis* BP1 extract. Biofilms that did not get extract treatment were utilized as a negative control. Following incubation, the acrylic in the microplate was rinsed twice with sterile PBS (Merck, Germany) and subjected to dehydration using a succession of ethanol solutions (70 % for 10 min, 95 % for 10 min, and 100 % for 20 min), air dried overnight. The lens covers were coated with Au (Hitachi MC1000 Au ion sputter, Japan). The coating process was done at a current of 10 mA for 60 s. The coated lens covers were then examined using SEM. SEM was used in high vacuum mode with an accelerating voltage of 5 kV. The spot intensity was set at 30 %, and magnifications of 500, 1,500, and 2,500 times were used [16,20].

Confocal laser scanning microscopy (CLSM) observation of *Candida albicans* biofilm cell death

CLSM was performed using the method in [20] with minor modifications. CLSM used a 96-well microplate. Biofilms were incubated using adverse control treatment, 50 and 100 µg mL^{-1} concentrations of BP1-P and BP1-S extracts, respectively, for 24 h. The biofilm formed at the bottom of the plate was washed with sterile PBS (Merck, Germany) and filled with 1,667 µg mL^{-1} fluorescein diacetate (FDA) and 500 µg mL^{-1} propidium iodide (PI), respectively, for 30 min and resuspended. Images were taken with a confocal microscope. Imaging of FDA and PI was performed with laser light at 488 and 555 nm, respectively, with 10x magnification. FDA is hydrolyzed by living cells, which results in the accumulation of green fluorescence, while PI stains dead cells red.

Characterization test Fourier transform infrared spectroscopy (FTIR)

FTIR characterization tests were performed using the protocol [21] with minor modifications. BP1-P and BP1-S extract samples were tested using FTIR in transmittance mode to determine the chemical groups present. The Nicolet 6,700 spectrometer was equipped with a deuterated triglycine sulfate (KBr) detector and a flexible Attenuated Total Reflectance (ATR) sample connection featuring a diamond crystal plate. The OMNIC 8.1 computer software was utilized to capture spectra within the 4,000 - 400 cm^{-1} spectral range. The spectral resolution was set at 4 cm^{-1}, with a gain of 2 samples and 32 sample/background scans.

Liquid chromatography-tandem mass spectrometry (LC-MS/MS) analysis

A total of 10 mg of BP1-P and BP1-S extracts were each diluted into 1 mL of methanol (LC-MS grade) and filtered using a 0.22 µm syringe filter. A Waters Acquity HPLC system (Waters, USA) performed reversed-phase liquid chromatography on the sample solution after being injected into an Eclipse Plus C18 RRHD column (2.1×100 mm, 1.8 µm; Waters, USA). The flow rate of the HPLC system was set at 0.4 mL min^{-1}. Water/0.01 % formic acid (A) and 100 % acetonitrile/0.01 % formic acid (B) were the mobile phases. Secondary metabolites were separated using a binary solvent elution gradient on the column for 20 min (0 min, 5 % B; 0 - 15 min, 5 - 100 % B; 15 - 17 min, 100 % B). The column was equilibrated at 5 % B for 3 min following injection. The electrospray voltage for positive ions is 3.9 kV, whereas the voltage for negative ions is 2.5 kV. In the LC-MS/MS process, the 5 most intense ions in each survey scan with a charge state of 1 and an ion number greater than 5,000 were chosen for MS/MS analysis through collision-induced dissociation (CID) in a linear ion trap or "higher-energy" collisional dissociation (HCD) in a collision cell in front of a C-trap. XCalibur 4.1.31.9 (Thermo Scientific, USA) was used to record and process raw data files [22].

Untargeted liquid chromatography-tandem high-resolution mass spectrometry (LC-HRMS)

The untargeted HRMS analysis employed 2 mobile phases, A: Distilled water with 0.1 % formic acid and B: Acetonitrile with 0.1 % formic acid. The analytical column utilized was the Hypersil Gold aQ column (50 ×1×1.9 mm^2 µm) (Thermo, USA). The flow rate was 40 µl min^{-1}, the sample injection volume was 5 µL, and the analysis gradient time was 30 min. The gradient was programmed with the following specifications: 2 min at 5 % B, 15 min at 60 % B, 22 min at 95 % B, 25 min at 95 % B, 25.1 min at 5 % B, and 30 min at 5 % B. The experiment involved conducting parallel reaction

monitoring at a resolution of 35,000 full widths at half maximum (FWHM). The procedure of heated electrospray ionization, namely positive ionization, and subsequent data processing was carried out using the XCalibur 4.1.31.9 (Thermo Scientific, USA) instrument [16].

***In silico* molecular docking**

This procedure refers to the reference [23] as follow:

Receptor preparation

The 3D structures of Als3 (PDB ID: 4LEE), Hwp1 (UniProt ID: Q14RS3), and Sap3 (PDB ID: 2H6T) adhesins from *C. albicans* were acquired from Protein Data Bank (https://www.rcsb.org/) and UniProt (https://www.uniprot.org/). The AutoDockTools-1.5.7 software (https://autodocksuite.scripps.edu/adt/) was employed to isolate the ligands and water molecules from the primary structure. Next, the structure was created by including polar hydrogen using the program.

Ligand preparation

The 3D structures of betaine, oleamide, l-phenylalanine, and l-pyroglutamic metabolite discovered in untargeted LC-HRMS investigations were obtained from the PubChem database (https://pubchem.ncbi.nlm.nih.gov/). The 3D structures were transformed utilizing PyMOL 4.6.0 software (https://pymol.org/). Subsequently, the AutoDockTools 1.5.7 program was employed to convert the initial ligand format.

Docking procedure

A .config file is compiled. The dimensions and position of the "grid box" are determined using AutoDockTools-1.5.7 software. The dimensions and centers of the grid box are adjusted to encompass all regions of the target protein. Subsequently, the essential data was documented and stored in the .config file, and an individualized .config file was generated for every ligand. The molecular docking results were evaluated using AutoDockTools-1.5.7 software. To thoroughly analyze the results, ligand-receptor complexes associated with the conformation that exhibited the greatest binding energy were prepared and evaluated for each compound using PyMOL 4.6.0 software. The visualization of these complexes was carried out using Discovery Studio 2021 Client software.

Statistical analysis

For antifungal, antibiofilm, and biofilm quantification, statistical analysis was performed on raw optical density data of 3 biological replicates, and the percentage of growth inhibition and biofilm formation of *C. albicans* was performed with two-way ANOVA using GraphPad Prism 10.1.2 (GraphPad Software, Inc., CA, USA) software. The results are presented as mean ± SD. All analyses with $p < 0.05$ were considered statistically significant.

Results and discussion

Antifungal and antibiofilm activity

To measure antifungal activity, various concentrations of the extract from *B. velezensis* BP1 (BP1-P and BP1-S) were co-incubated with *C. albicans* for 24 h. BP1-P and BP1-S extract demonstrated inhibitory activity against *C. albicans*, as demonstrated by their respective MIC_{50} values of 94.49 and 93.81 μg mL^{-1} following a 24-hour treatment period that indicate the concentration required to inhibit 50 % of planktonic (free-floating) *C. albicans* growth, according to the results of the assay. At doses ranging from 50 to 400 μg mL^{-1}. **Figure 1(A)** demonstrates the antifungal efficacy of BP1-P and BP1-S *B. velezensis* BP1 extracts against *C. albicans*. Significant differences were seen at doses of 50 - 400 μg mL^{-1} in all types of extracts when compared to the extract-free control group ($p < 0.05$), according to statistical analysis (two-way ANOVA, *p*-value = 0.05). These results (**Figure 1(B)**) for antifungal activity were comparable to those for reducing biofilm concentration. There was a decrease in biofilm concentration (OD_{490}) at all concentration levels of BP1-P and BP1-S extracts (25 - 400 μg mL^{-1}). A two-way ANOVA analysis showed that all extract concentrations compared to the untreated control had significant differences ($p < 0.05$), for BP1-P and BP1-S extract concentrations of 100 μg mL^{-1}, biofilm suppression levels of approximately 28 and 30 % were observed ($p < 0.001$).

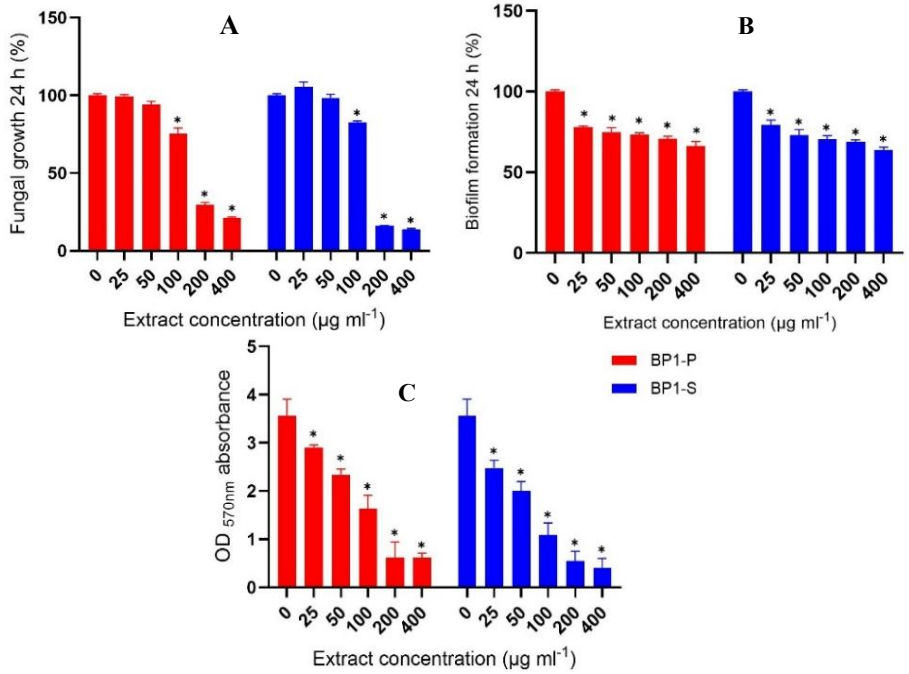

Figure 1 Antifungal activity (A), biofilm formation at 24 h of incubation times (B), and biofilm concentration at 24 h of incubation times (C) BP1-P and BP1-S extracted from *B. velezensis* BP1 against *C. albicans* ATCC 10230. Values are expressed as the mean SD of 3 replicates (*$p < 0.001$).

Figure 1(C) shows that the biofilm maturation analysis results in 24 h after biofilm formation by crystal violet staining were comparable to the decrease in antifungal and biofilm concentrations. All concentrations of BP1-P and BP1-S extract demonstrated reduced biofilm development compared to the extract-free control during a 24-hour maturation period. After 24 h, biofilm formation varied significantly across all concentration levels and extract types, according to the results of the two-way ANOVA test. The control group did not incorporate any extract. After applying extract concentrations of 50 and 100 µg mL^{-1}, the average absorbance at 570 nm in the control group was lowered to 2.13 and 1.33 (BP1-P), 2.00 and 1.08 (BP1-S), respectively. All the data suggest that the treatment with *B. velezensis* BP1 extract interrupted biofilm formation, which decreased as the extract concentration rose. Utilizing confocal laser scanning microscopy (CLSM) and scanning electron microscopy (SEM) at a concentration of 100 µg mL^{-1}, these concentration levels of BP1-P and BP1-S extracts were utilized to analyze biofilm formation.

Biofilm production is a prominent marker of infection, characterized by the formation of a complex multicellular structure by *C. albicans* that can lead to both mucosal and systemic illnesses [24]. In this study, the investigation demonstrated that BP1-P and BP1-S extract had antifungal and antibiofilm properties against *C. albicans*. The antifungal activity was most pronounced at a concentration of 100 - 400 µg mL^{-1} (**Figure 1(A)**), comparable to the lowest concentration required for biofilm development (**Figure 1(B)**). Biofilm formation reached maturity within 24 h of incubation (**Figure 1(C)**). The use of 100 µg mL^{-1} concentration exhibited similarity to the biofilm development investigation conducted using SEM (**Figure 2**) and the biofilm development analysis using CLSM (**Figure 3**).

Biofilm development is a prominent indicator of *C. albicans* infection. Biofilms are intricate structures composed of many cells created by *C. albicans* that adhere to the surfaces of living cells. These are three-dimensional arrays of *C. albicans* consisting of intricate cell assemblies coupled to host tissues or abiotic surfaces and surrounded by extracellular polysaccharides (EPS) [24,25]. *In vitro* research conducted [4], showed that the biofilm is formed after 24 h and its development increases as the incubation time increases.

Inhibition of biofilm formation

To compare the effects of BP1-P and BP1-S extracts with the control treatment (no extract) in inhibiting *C. albicans* biofilm formation, BP1-P and BP1-S extracts at concentrations of 100 µg mL^{-1} (SEM, 48 h incubation) and 50 - 100 µg mL^{-1} (CLSM, 24 h incubation) were used. Incorporating extracts can effectively impede the development of *C. albicans* biofilm. Without the extract, the cells subjected to the control treatment exhibited robust and densely populated growth with a uniform and smooth colony cell shape (**Figure 2(A)**). Cells that were not treated exhibited significant differences compared to cells that were treated with various extracts. The treated cells had minimal cell proliferation, irregular form, rough surface, and disrupted hyphae (**Figures 2(B) - 2(C)**). The scanning electron microscopy (SEM) examination revealed a decrease in the density of biofilm cells, with a significant concentration of cells observed only during the hyphae development stage (proliferation stage). The treatment using an extract concentration of 100 µg mL^{-1} did not exhibit elongated hyphae (red arrow, **Figure 2(C)**). This suggests that the metabolite extract from *B. velezensis* BP1 hindered the creation of biofilms by impeding elongation and causing damage to the structure and production of hyphae.

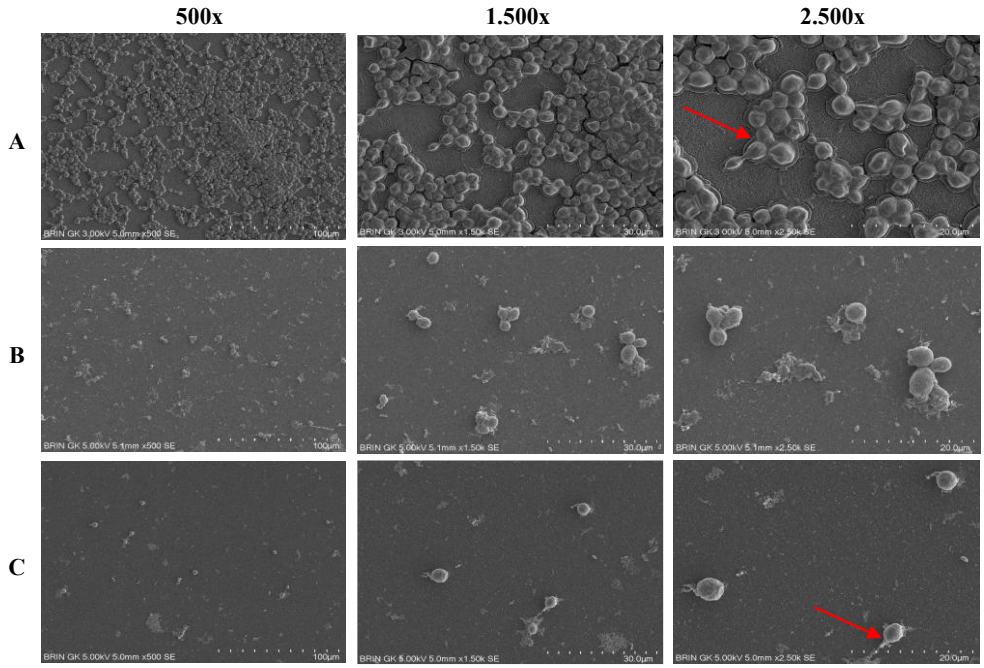

Figure 2 Scanning electron microscope (SEM) (1) biofilm formation of *C. albicans* ATCC 10230 on RPMI medium control (A); with 100 µg mL^{-1} treatment of *B. velezensis* BP1-P (B); and BP1-S extracts (C). Each treatment group was visualized at 500x, 1,500x, and 2,500x magnification.

The CLSM analysis of *C. albicans* biofilm in the control group without extracts revealed that all cells were viable, with no instances of cell death (**Figure 3(A)**). The biofilm formation was disturbed in the BP1-P and BP1-S extract treatment groups, with the extent of inhibition dependent on the concentration of the extract (**Figures 3(B) - 3(E)**). Following the extraction procedure, the vitality of the hyphae was diminished, as observed through the use of fluorescein diacetate (FDA) labeling, leading to the accumulation of green fluorescence. The percentage of deceased hyphae exhibited a notable rise, as demonstrated by the red propidium iodide (PI) labeling. However, this increase was particularly significant in the treatment with an extract concentration of 100 µg mL^{-1}, as determined through analysis using confocal laser scanning microscopy (CLSM) (**Figures 3(C)** and **3(E)**).

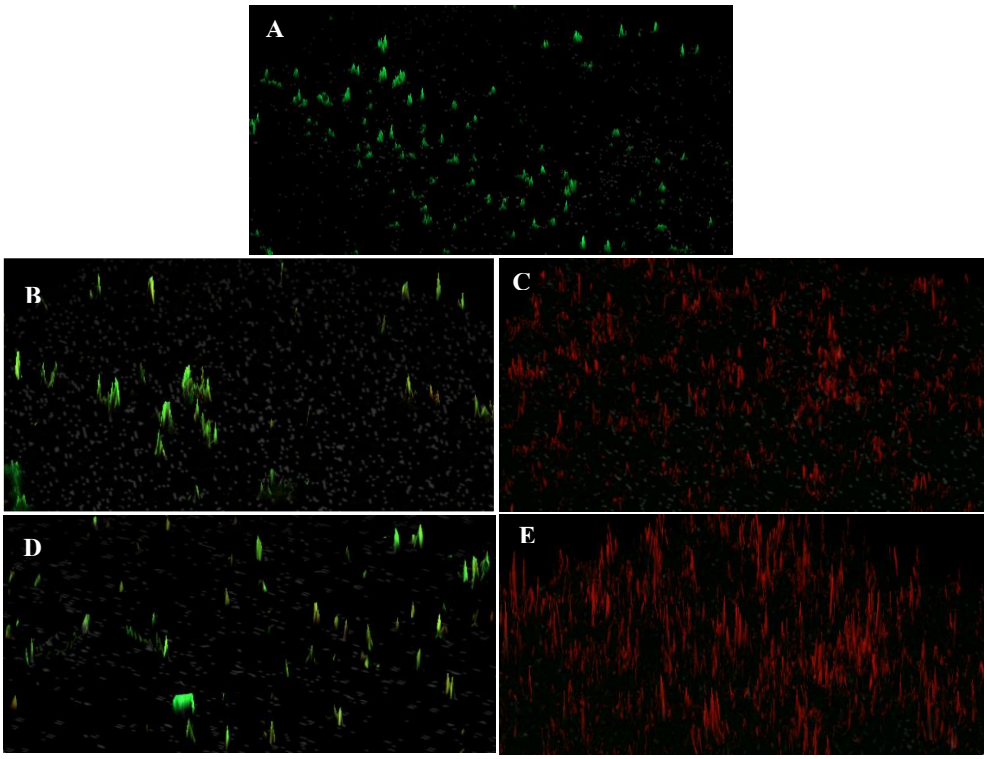

Figure 3 Confocal laser scanning microscopy (CLSM). Biofilm formation of *C. albicans* on RPMI medium control (A); group treated with 50 µg mL^{-1} BP1-P (B); group treated with 100 µg mL^{-1} BP1-P (C); group treated with 50 µg mL^{-1} BP1-S (D); group treated with 100 µg mL^{-1} BP1-S (E). FDA is hydrolyzed by living cells and results in the accumulation of green fluorescence, while PI stains dead cells and is colored red.

The development of *C. albicans* biofilms is often influenced by multiple creation stages, including adhesion, proliferation, maturation, and dispersion [7]. During the adhesion stage, cells of *C. albicans* attach themselves to the substrate to create a basal layer of cells. During the proliferation stage, cells undergo elongation and differentiate into hyphae. During the maturation stage, the secretion of EPS (extracellular polymeric substances) takes place as hyphae (filamentous structures) are formed [26]. *C. albicans* cells experience a loss of capacity to proliferate, resulting in low cell growth. Consequently, they cannot progress to maturation and biofilm production (**Figure 2**). These results indicate that extracts BP1-P and BP1-S can inhibit biofilm formation by inhibiting the proliferation stage. The mechanism of inhibition of pathogenic fungi by *Bacillus* spp. metabolite compounds are divided into cell walls, membrane damage, and intracellular damage. The compounds synthesize target cell wall components through a complex mechanism that can kill target cells by stopping cell respiration and extracellular membrane protein synthesis and altering the physiological functions of pathogenic fungi [12].

Characterization of FTIR

BP1-P and BP1-S extracts showed specific FTIR spectrum profiles. In the BP1-P extract, O-H and C-O stretching vibrations were seen, C = O and CO-O-CO stretching vibrations in BP1-S, and both extracts C = C, N-O, C-N, and C-Cl stretching vibrations and symmetrical C-H stretching vibrations from the CH2 group bond were seen. The FTIR spectrum of BP1 extracts with its phenolic content (**Figure 4**).

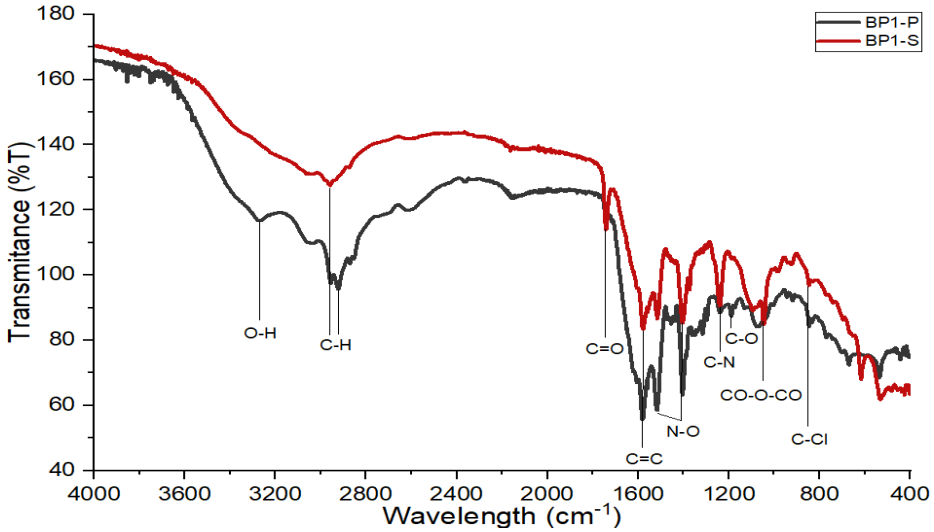

Figure 4 FTIR spectra of *B. velezensis* BP1-P (black line) and BP1-S extracts (red line).

BP1-P and BP1-S extracts underwent additional analysis using FTIR to identify the functional groups in the extracts. FTIR is an analytical technique employed to detect and describe the chemical compounds present in a sample by analyzing the absorption of infrared spectra [27,28]. **Figure 4** displays the FTIR spectrum of the BP1 extract together with its phenolic content. The wavelength of 1,522.09 cm^{-1} is caused by the stretching of N-H bonds in hydrogen bonds and the potential binding of metals to amide groups in proteins found in cells. The existence of peptide components is indicated by the C-H stretching vibrations typical of alkyl chains, observed at 2,598 - 3,199 cm^{-1}. The peak at 1,026 - 1,241 cm^{-1} corresponds to the presence of amide functional groups [29]. Aliphatic chains can be inferred from the absorption peak at 2,936 cm^{-1}, attributed to C-H stretching [30].

Main constituents of active metabolites

LC-MS/MS analysis results detected 3 compounds from the BP1-P extract and 2 from the BP1-S extract using MS/MS spectra (**Figure 5**). Then, untargeted LC-HRMS analysis of BP1-P extract resulted in 266 compounds, and BP1-S extract resulted in 273 compounds in the form of metabolite compounds and amino acids. The twenty highest compounds with the most significant area and mzCloud best match above 70 % for BP1-P and BP1-S (**Table 1** and Supplementary Material). The highest compounds detected in BP1-P are betaine and oleamide; in BP1-S are l-phenylalanine and l-pyroglutamic compounds, which are known to have potential as antifungals. This study shows that betaine, oleamide, l-phenylalanine, and l-pyroglutamic produced by *B. velezensis* BP1 have enormous potential as antifungal and antibiofilm agents against *C. albicans*.

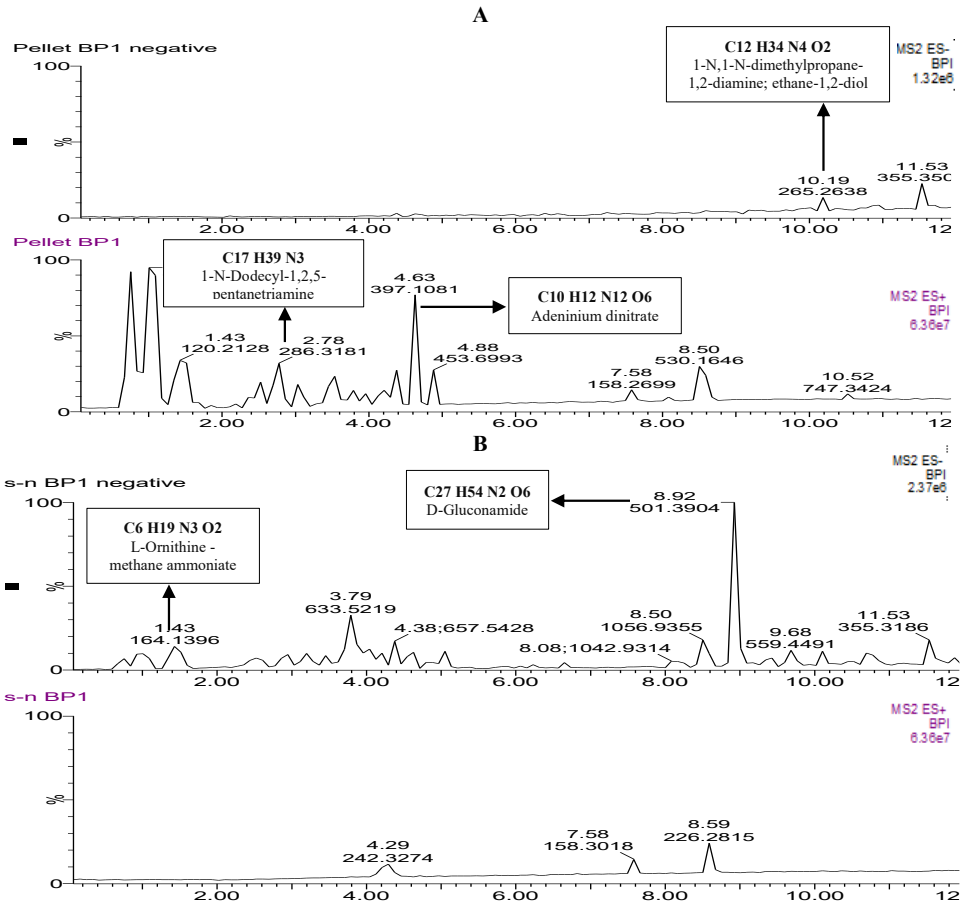

Figure 5 LC-MS/MS analysis of BP1-P (A) and BP1-S extracts (B) with positive and negative ion modes.

D-Gluconamide compounds detected in BP1-S extract (**Figure 5(B)**) from LC-MS/MS analysis have been shown to inhibit the growth of various fungal species, including *C. albicans* [31]. D-gluconamide has been found to effectively suppress biofilm formation in the fungus *C. albicans* [32]. To detect compounds in the extracts, further metabolite profiling analysis was performed using untargeted LC-HRMS (**Table 1** and Supplementary Material). The study revealed a rich profile of metabolite compounds and amino acids in BP1-P and BP1-S extracts, including betaine, oleamide, l-phenylalanine, and l-pyroglutamic, which showed antifungal properties. The antifungal activity of herbal toothpaste containing betaine derivatives showed significant Inhibition against *C. albicans* [33].

Oleamide compounds were also shown to be involved in antifungal activity against various fungal species, including *Aspergillus flavus* and *Fusarium oxysporum*, related to their ability to inhibit the growth of these fungi [34,35]. Furthermore, l-phenylalanine treatment significantly reduced the decayed area caused by various pathogenic fungi, including *Colletotrichum*, *Aspergillus*, and *Lasiodiplodia*, on mango and avocado fruits [36]. In addition, another compound detected by LC-HRMS untargeted metabolite profiling analysis, l-pyroglutamic, can be an antifungal on *Fusarium graminearum* and *Alternaria alternariae* [37]. Our findings suggest that BP1-P and BP1-S extracts can synthesize various metabolite compounds and amino acids that have the potential as antifungals such as d-gluconamide, oleamide, l-phenylalanine and l-pyroglutamic which will be further analyzed by molecular docking.

Molecular docking studies

Molecular docking was conducted on 4 specific compounds derived from the BP1-P and BP1-S extract. This was done as part of an untargeted LC-HRMS screening to assess their affinity and binding mechanism with 3 target proteins: Agglutinin-Like Sequence 3 (ALS3), Hyphal Wall Protein 1 (HWP1), and Secreted Aspartic Proteinase 3 (SAP3). The chemical and the target protein were subjected to molecular docking to assess their bond compatibility. The docking results

revealed that the 4 phenolic compounds showed good binding in the catalytic pocket of the 3 proteins tested. Visualization in 2D and 3D to see the interaction between the ligand and the active side of the target protein (**Figure S(1)**). Specific molecules were selected based on their prominent differential inhibition scores (**Table 2**).

Table 2 Molecular docking results of some compounds from LC-HRMS analysis with ALS3, HWP1, and SAP3 protein target.

Protein target	Compound/ ligand	Afinitas (kcal mol^{-1})	RMSD (Å)	Hydrophobic interactions (Alkyl and Pi-Alkyl)	Hydrogen interactions
ALS3	Betaine	–3.5	0.899	-	Phe60
	Oleamide	–5.2	1.067	Val161, Tyr23, Tyr21	Thr296
	L-Phenylalanine	–5.6	1.248	Arg171, Val116, Pro29	Thr296, Phe298
	L-Pyroglutamic	–4.9	0.966	-	Asp169, Trp224, Ser159, Asn225
	Fluconazole*	–7.3	1.222	Met59, Val172, Pro29, Arg171	-
HWP1	Betaine	–3.8	0.869	-	-
	Oleamide	–5.1	1.655	Met164, Tyr161, Lys172	Asn43, Arg176
	L-Phenylalanine	–6.9	0.994	Ala100, Ile96	Tyr57, Ser124
	L-Pyroglutamic	–5.5	0.359	-	Asp66, Ile96
	Fluconazole*	–6.4	1.044	Lys16	Asn12, Ser48
SAP3	Betaine	–3.6	1.156	-	Thr88
	Oleamide	–5.6	1.192	Val30, Tyr84, Ile123, Val12	Thr222, Ile223
	L-Phenylalanine	–6.0	1.381	Val30	Asp86, Val12, Thr222
	L-Pyroglutamic	–4.9	1.146	-	Asn192, Tyr128, Thr130, Ser36, Lys129
	Fluconazole*	–6.9	1.019	Val30, Val119, Ile123	Asp86

The study found that the BP1-P and BP1-S extracts exhibited potent inhibition against ALS3, HWP1, and SAP3 proteins. This inhibition was attributed to the presence of phenolic chemicals produced by bacteria. The specific details may be found (**Table 2**). ALS3 is a protein produced by opportunistic fungi that has a crucial function in the attachment, establishment, and disease-causing stages of *C. albicans* [23]. HWP1 is a protein produced during the initial phases of biofilm formation. It encodes a fungal cell wall protein necessary for hyphae's growth and the adhesion of *C. albicans* cells to host epithelial cells [38]. SAP3 is a virulence factor that plays a role in several stages of *C. albicans* infection. It breaks down molecules to acquire nutrients and alters the host cell membrane to promote adhesion and tissue invasion [39].

The binding energy between ALS3 protein from *C. albicans* with betaine, oleamide, l-phenylalanine, and l-pyroglutamic compounds with a binding energy of –3.5, –5.2, –5.6, and –4.9 kcal mol^{-1}. Then, the binding energy between the HWP1 protein and similar compounds with binding energies of –3.8, –5.1, –6.9, and –5.5 kcal mol^{-1}. The binding energy between SAP3 protein and similar compounds resulted in binding energies of –3.6, –5.6, –6.0, and –4.9 kcal mol^{-1} (**Table 2**). The four compounds have more incredible binding energy compared to the standard antifungal ligand compound fluconazole (–7.3, –6.4, –6.9 kcal mol^{-1}) but with a slight difference, except for the compound l-phenylalanine with HWP1 protein

which has a smaller affinity value. The smaller the binding energy value in molecular docking results, the smaller the energy that binds to the protein, so the ligand compound binds/inhibits the target protein [40].

Regarding molecular docking analysis on ALS3 protein (**Figure 1(S)** and **Table 2**), betaine inhibits by forming hydrogen bonds with amino acid Phe60. Oleamide compounds by forming hydrophobic bonds with amino acids Val161, Tyr23, and Tyr21 and forming hydrogen bonds with amino acid Thr296. L-Phenylalanine inhibits by forming hydrophobic bonds with Arg171, Val116, and Pro29 and hydrogen bonds with amino acids Thr296 and Phe298. Also, l-pyroglutamic compounds inhibit ALS3 by forming hydrogen bonds with amino acids Asp169, Trp224, Ser159, and Asn225.

In docking analysis on the HWP1 protein (**Figure 1(S)** and **Table 2**), betaine does not form hydrophobic or hydrogen bonds. Oleamide compounds are inhibited by forming hydrophobic bonds with Met164, Tyr161, and Lys172 and hydrogen bonds with amino acids Asn43 and Arg176. L-phenylalanine is inhibited by forming hydrophobic bonds with Ala100 and Ile96 and hydrogen bonds with amino acids Tyr57 and Ser124. Also, l-pyroglutamic compounds inhibit ALS3 by forming hydrogen bonds with amino acids Asp66 and Ile96.

Then, in molecular docking analysis on SAP3 protein (**Figure 1(S)** and **Table 2**), betaine is inhibited by forming hydrogen bonds with the amino acid Thr88. Oleamide compounds by forming hydrophobic bonds with amino acids Val30, Tyr84, Ile123, and Val12 and forming hydrogen bonds with amino acids Thr222 and Ile223. L-phenylalanine is inhibited by forming hydrophobic bonds with Val30 and hydrogen bonds with amino acids Asp86, Val12, and Thr222. Moreover, l-pyroglutamic compounds inhibit ALS3 by forming hydrogen bonds with amino acids Asn192, Tyr128, Thr130, Ser36, and Lys129.

Results of molecular docking and visualization of hydrogen bonds, as well as alkyl and pi-alkyl (hydrophobic) bonds, show that the 4 secondary metabolite compounds of *B. velezensis* BP1 can bind well to ALS3, HWP1, and SAP3 proteins. The bond causes inhibition/inhibition of the target protein to inhibit the growth and formation of biofilms on *C. albicans*. Hydrogen bonds indicate a strong interaction between metabolites and protein targets. Hydrogen bonds are essential for stabilizing ligand-protein complexes and can increase the efficacy of metabolites as potential inhibitors [41]. Then, hydrophobic bonds contribute to the binding affinity of the metabolite. This interaction involves the hydrophobic region of the protein, which can increase the overall stability of the complex formed during binding [41,42]. Thus, hydrogen and hydrophobic bonds in the docking results indicate that the four *B. velezensis* BP1 compounds tested have significant potential for *C. albicans* antibiofilm applications.

Molecular docking results are validated to determine the standard deviation value of the docking simulation performed; the validation is done using Root Mean Standard Deviation (RMSD) analysis, which is the standard deviation value between the prediction and the actual value. RMSD value on docking simulation of ≤ 2Å can be interpreted as a stable docking model and resembles the real interaction [43]. The smaller the RMSD value between 2 structures, the more similar the structures will be [40]. Four compounds from the extract of *B. velezensis* BP1 showed RMSD values ≤ 2Å, so the *in silico* molecular docking analysis conducted in this study can be said to be stable and able to resemble the interaction of compounds against the natural target proteins ALS3, HWP1, and SAP3. Despite being demonstrated in laboratory experiments and *in silico* molecular docking studies, the precise way in which the molecule works, particularly in the communication process of biofilm formation known as quorum sensing, needs additional investigation to establish the optimal dosage for its effectiveness as an antifungal and antibiofilm agent.

Conclusions

This study shows that BP1-P and BP1-S extract from *B. velezensis* BP1 can inhibit planktonic cell growth and biofilm formation of *C. albicans* based on antifungal, antibiofilm, and biofilm quantification activity tests *in vitro*. This study has discovered novel secondary metabolites and amino acids generated by the bacteria *B. velezensis* BP1 with potential as antifungal agents. Betaine, oleamide, l-phenylalanine, and l-pyroglutamic acid could be alternate antifungal and antibiofilm agents against the biofilm-forming fungi *C. albicans*. Based on *in silico* molecular docking studies,

the betaine, oleamide, l-phenylalanine, and l-pyroglutamic compounds synthesized by *B. velezensis* BP1 were confirmed to be able to interact with ALS3, HWP1, and SAP3 proteins that play a role in *C. albicans* biofilm formation.

Acknowledgments

The authors thank the Universitas Gadjah Mada, Indonesia, for being supported by the Final Project Recognition, Grant ID 4971/UN1.P1/PT.01.01/2024. The authors also thank The Directorate of Laboratory Management, Research Facilities and Science and Technology Park, National Research and Innovation Agency (BRIN) Yogyakarta, Indonesia, for providing SEM and LC-HRMS facilities through ELSA BRIN services.

References

[1] K Kainz, MA Bauer, F Madeo and D Carmona-Gutierrez. Fungal infections in humans: The silent crisis. *Microbial Cell* 2020; **7(6)**, 143-145.

[2] IU Macias-Paz, S Pérez-Hernández, A Tavera-Tapia, JP Luna-Arias, JE Guerra-Cárdenas and E Reyna-Beltrán. *Candida albicans* the main opportunistic pathogenic fungus in humans. *Revista Argentina de Microbiología* 2023; **55(2)**, 189-198.

[3] J Talapko, M Juzbašić, T Matijević, E Pustijanac, S Bekić, I Kotris and I Škrlec. *Candida Albicans* - the virulence factors and clinical manifestations of Infection. *Journal of Fungi* 2021; **7(2)**, 79.

[4] S Desrini, M Girardot, C Imbert, M Mustofa and T Nuryastuti. Screening antibiofilm activity of invasive plants rowing at the slope Merapi mountain, central Java, against *Candida albicans*. *BioMed Central Complementary Medicine and Therapies* 2023; **23(1)**, 232.

[5] M Cavalheiro and MC Teixeira. *Candida* biofilms: Threats, challenges, and promising strategies. *Frontiers in Medicine* 2018; **5**, 28.

[6] RM Pereira, D Sandri, GFA Rios and DAO Sousa, Automation of irrigation by electronic tensiometry based on the arduino hardware platform. *Revista Ambiente & Água* 2020; **15(4)**, 1-12.

[7] W Wang, J Zhao and Z Zhang. *Bacillus* metabolites: Compounds, identification and anti-*Candida albicans* mechanisms. *Microbiology Research* 2022; **13(4)**, 972-984.

[8] SS Chew, LTH Tan, JWF Law, P Pusparajah, BH Goh, NSA Mutalib and H Lee. Targeting gut microbial biofilms: A key to hinder colon carcinogenesis. *Cancers* 2020; **12(8)**, 2272.

[9] S Singh and R Shalini. Effect of hurdle technology in food preservation: A review. *Critical Reviews in Food Science and Nutrition* 2014; **56(4)**, 641-649.

[10] C Nannan, HQ Vu, A Gillis, S Caulier, TTT Nguyen and J Mahillon. Bacilysin within the *Bacillus subtilis* group: Gene prevalence versus antagonistic activity against gram-negative foodborne pathogens. *Journal of Biotechnology* 2021; **327**, 28-35.

[11] D Miljaković, J Marinković and S Balešević-Tubić. The significance of *Bacillus* spp. In disease suppression and growth promotion of field and vegetable crops. *Microorganisms* 2020; **8(7)**, 1037.

[12] C Tran, IE Cock, X Chen and Y Feng. Antimicrobial *Bacillus*: Metabolites and their mode of Action. *Antibiotic* 2022; **11(1)**, 88.

[13] LK Caesar, R Montaser, NP Keller and NL Kelleher. Metabolomics and genomics in natural products research: Complementary tools for targeting new chemical entities. *Natural Product Reports* 2021; **38(11)**, 2041-2065.

[14] X Chu, M Jaeger, J Beumer, OB Bakker, R Aguirre-Gamboa, M Oosting, SP Smeekens, S Moorlag, VP Mourits, VACM Koeken, CD Bree, T Jansen, IT Mathews, K Dao, M Najhawan, JD Watrous, I Joosten, S Sharma, HJPM Koenen, S Withoff, …, Y Li. Integration of metabolomics, genomics, and immune phenotypes reveals the causal roles of metabolites in disease. *Genome Biology* 2021; **22(11)**, 198.

[15] G Chen, AJ Seukep and M Guo. Recent advances in molecular docking for the research and discovery of potential *Marine Drugs*. *Marine Drugs* 2020; **18(11)**, 545.

[16] H Nirwati, E Damayanti, EN Sholikhah, M Mutofa and J Widada. Soil-derived *Streptomyces* sp. GMR22 producing antibiofilm activity against *Candida albicans*: bioassay, untargeted LC-HRMS, and gene cluster analysis. *Heliyon* 2022; **8(4)**, 09333.

[17] MD Rakhmawatie, N Marfuati, B Barsaliputri, AZ

Fikriyah and SN Ethica. Antibacterial activity and GC-MS profile of secondary metabolites of *Bacillus subtilis* subsp. *subtilis* HSFI-9 associated with Holothuria scabra, Biodiversitas. *Journal of Biological Diversity* 2023; **24(5)**, 2843-2849.

[18] F Masmoudi, NS Pothuvattil, S Tounsi, I Saadaoui and M Trigui. Synthesis of silver nanoparticles using *Bacillus velezensis* M3-7 lipopeptides: Enhanced antifungal activity and potential use as a biocontrol agent against *Fusarium* crown rot disease of wheat seedlings. *International Journal of Food Microbiology* 2023; **407**, 110420.

[19] Y Dabiré, NS Somda, CS Compaoré, I Mogmenga, MK Somda, AS Ouattara, MH Dicko, JO Ugwuanyi, LI Ezeogu and AS Traoré. Molecular screening of bacteriocin-producing *Bacillus* spp. isolated from Soumbala, a fermented food condiment from Parkia biglobosa seeds. *Scientific African* 2021; **12**, 00836.

[20] RH Liu, ZC Shang, TX Li, MH Yang and LY Kong. *In vitro* antibiofilm activity of eucarobustol E against *Candida albicans*. *Antimicrobial Agents and Chemotherapy* 2017; **61(8)**, 02707-02716.

[21] D Kowalczuk and M Pitucha. Application of FTIR method for the assessment of immobilization of active substances in the matrix of biomedical materials. *Materials* 2019; **12(18)**, 2972.

[22] I Shahid, J Han, S Hanooq, KA Malik, CH Borchers and S Mehnaz. Profiling of metabolites of *Bacillus* spp. and their application in sustainable plant growth promotion and biocontrol. *Frontiers in Sustainable Food Systems* 2021; **5**, 605195.

[23] YS Ahrabi and SN Khoei. Investigation of some natural products as an inhibitor of Agglutinin-Like Sequence (Als3) from *Candida albicans* (Skin Candidiasis): An in-silico study. *Journal of Skin and Stem Cells* 2023; **10(4**), 142360.

[24] D Sharma, L Misba and AU Khan. Antibiotics versus biofilm: An emerging battleground in microbial communities, antimicrobial resistance & amp. *Infection Control and Hospital Epidemiology* 2019; **8**, 76.

[25] I Martin, V Waters and H Grasemann. Approaches to targeting bacterial biofilms in cystic fibrosis airways. *International Journal of Molecular Sciences* 2021; **22(4)**, 2155.

[26] V Amann, AK Kissmann, M Krämer, I Krebs, JA Perez-Erviti, AJ Otero-Gonzalez, F Morales-Vicente, A Rodríguez, L Ständker, T Weil and F Rosenau. Increased activities against biofilms of the pathogenic yeast *Candida albicans* of optimized Pom-1 derivatives. *Pharmaceuticals* 2022; **14(2)**, 318.

[27] Y Cai, C Zhai, X Yu, Y Sun, J Xu, Y Zheng, Y Cong, Y Li, A Chen, H Xu, S Wang and X Wu. Quantitative characterization of water transport and wetting patterns in coal using LF-NMR and FTIR techniques. *Fuel* 2023; **350**, 128790.

[28] W Zhang, A Fina, G Ferraro and R Yang. FTIR and GCMS analysis of epoxy resin decomposition products feeding the flame during UL 94 standard flammability test: Application to the understanding of the blowing-out effect in epoxy/polyhedral silsesquioxane formulations. *Journal of Analytical and Applied Pyrolysis* 2018; **135**, 271-280.

[29] OB Akpor, OD Akinwusi and TA Ogunnusi. Production, characterization and pesticidal potential of *Bacillus* species metabolites against sugar ant (Camponotus consobrinus). *Heliyon* 2021; **7(11)**, 08447.

[30] ASA Al-Thubiani, YA Maher, A Fathi, MAS Abourehab, M Alarjah, MSA Khan and SB Al-Ghamdi. Identification and characterization of a novel antimicrobial peptide compound produced by *Bacillus megateriumstrain* isolated from oral microflora. *Saudi Pharmaceutical Journal* 2018; **26(8)**, 1089-1097.

[31] J Cardoso, DG Nakayama, E Sousa and E Pinto. Marine-derived compounds and prospects for their antifungal application. *Molecules* 2020; **25(24)**, 5856.

[32] L Camaioni, B Ustyanowski, M Buisine, D Lambert, B Sendid, M Billamboz and S Jawhara. Natural compounds with antifungal properties against *Candida albicans* and identification of Hinokitiol as a promising antifungal drug. *Antibiotics* 2023; **12(11)**, 1603.

[33] G Adwan, Y Salameh, K Adwan and A Barakat. Assessment of antifungal activity of herbal and conventional toothpastes against clinical isolates of *Candida albicans*. *Asian Pacific Journal of Tropical Biomedicine* 2012; **2(5)**, 375-379.

[34] P Scano, MB Pisano, A Murgia, S Cosentino and P Caboni. GC-MS metabolomics and antifungal

characteristics of autochthonous *Lactobacillus* strains. *Dairy* 2021; **2(3)**, 326-335.

[35] Q Peng, J Yang, Q Wang, H Suo, AM Hamdy and J Song. Antifungal effect of metabolites from a new strain *Lactiplantibacillus Plantarum* LPP703 isolated from naturally fermented Yak Yogurt. *Foods* 2023; **12(1)**, 181.

[36] MK Patel, D Maurer, O Feygenberg, A Ovadia, Y Elad, M Oren-Shamir and N Alkan. Phenylalanine: A promising inducer of fruit resistance to postharvest pathogens. *Foods* 2020; **9(5)**, 646.

[37] L Ai, S Fu, Y Li, M Zuo, W Huang, J Huang, Z Jin and Y Chen. Natural products-based: Synthesis and antifungal activity evaluation of novel L-pyroglutamic acid analogues. *Frontiers in Plant Science* 2022; **13**, 1102411.

[38] FEZ Fathy, Y Ahmed and SA Salam. Hyphal wall protein 1 gene and biofilm formation among *Candida albicans* isolates from Ain Shams University Hospitals. *Egyptian Journal of Medical Microbiology* 2023; **32(1)**, 163-168.

[39] AT Permata, AA Prasetyo and S Haryati. Molecular analysis of *Candida albicans* Secreted Aspartyl Proteinase 3 (SAP3) Indonesian isolate. *IOP Conference Series: Materials Science and Engineering* 2018; **434**, 012112.

[40] EM Terefe and A Ghosh. Molecular docking, validation, dynamics simulations, and pharmacokinetic prediction of phytochemicals isolated from *Croton dichogamus* against the HIV-1 reverse ranscriptase. *Bioinformatics and Biology Insights* 2022; **16**, 11779322221125605.

[41] FA Ugbe, GA Shallangwa, A Uzairu and I Abdulkadir. Molecular docking screening and pharmacokinetic studies of some Boron-Pleuromutilin analogues against possible targets of *Wolbachia pipientis*. *Journal of Molecular Docking* 2022; **2(1)**, 29-43.

[42] M Yildirim and I Celik. *Applications of molecular docking studies in SARS-CoV-2 targeted drug discovery and the gains achieved through molecular docking*. IntechOpen, London, 2024.

[43] H Hamzah, T Nuryastuti, W Rahmah, L Chabib, ES Syamsul, D Lestari, A Jabbar and SUT Pratiwi. Molecular docking study of the C-10 Massoia Lactone compound as an antimicrobial and antibiofilm agent against *Candida tropicalis*. *The Scientific World Journal* 2023; **2023**, 6697124.

Supplementary Material

Table 1 The main constituents of BP1-P and BP1-S detected using untargeted liquid chromatography-tandem high-resolution mass spectrometry (LC-HRMS).

BP1-P Extracts						
Name of compound	**Formula**	**Molecular weight**		**RT [min]**	**Area (Max.)**	**mzCloud best match**
		Calculation	**Reference**			
Betaine	$C_5H_{11}NO_2$	117.07	117.15	0.89	24.268.809.542	94.2
Oleamide	$C_{18}H_{35}NO$	281.27	281.5	14.935	5.582.130.875	99.3
trans-3-Indoleacrylic acid	$C_{11}H_9NO_2$	187.06	187.19	2.314	3.916.335.472	93.3
D-(+)-Proline	$C_5H_9NO_2$	115.06	115.13	0.9	3.545.504.027	99.7
3-(propan-2-yl)-octahydropyrrolo [1,2a] pyrazine-1,4-dione	$C_{10}H_{16}N_2O_2$	196.12	196.25	3.884	2.782.731.315	97.6
Leucylproline	$C_{11}H_{20}N_2O_3$	228.14	228.29	2.454	1.971.661.034	98.5
Valylproline	$C_{10}H_{18}N_2O_3$	214.13	214.26	1.28	1.645.287.344	97.2
Cyclo(phenylalanyl-prolyl)	$C_{14}H_{16}N_2O_2$	244.12	454.60	6.101	1.283.133.430	97.9
Erucamide	$C_{22}H_{43}NO$	337.33	337.6	16.931	1.193.342.916	97.1
L-Isoleucine	$C_6H_{13}NO_2$	131.09	131.17	0.991	894.455.770	99.8
Hexadecanamide	$C_{16}H_{33}NO$	255.26	255.44	14.501	860.330.353.8	98
3-[(4-hydroxyphenyl)methyl]-octahydropyrrolo[1,2-a]pyrazine-1,4-dione	$C_{14}H_{16}N_2O_3$	260.11	260.29	3.926	735.076.546.9	98.5
L-Glutamic acid	$C_5H_9NO_4$	147.05	147.13	0.901	688.773.720.2	99.7
2-Amino-1,3,4-octadecanetriol	$C_{18}H_{39}NO_3$	317.29	317.5	10.038	575.261.546.9	83.7
3-(1-hydroxyethyl)-2,3,6,7,8,8a-hexahydropyrrolo[1,2-a]pyrazine-1,4-dione	$C_9H_{14}N_2O_3$	198.11	198.22	1.419	495.585.255.8	96.7

BP1-P Extracts						
Name of compound	**Formula**	**Molecular weight**		**RT [min]**	**Area (Max.)**	**mzCloud best match**
		Calculation	**Reference**			
Stearamide	$C_{18}H_{37}NO$	283.28	283.5	15.622	463.860.436.4	99.8
2,6-Pyridinecarboxylic acid	$C_7H_5NO_4$	167.02	-	1.579	399.358.042.2	94.1
Hypoxanthine	$C_5H_4N_4O$	136.03	136.11	1.095	370.350.900.4	99.6
L-Histidine	$C_6H_9N_3O_2$	155.06	155.15	0.833	323.068.153.4	99.9
N,N-Diisopropylethylamine (DIPEA)	$C_8H_{19}N$	129.15	129.24	3.241	300.091.306.2	73.7
L-Phenylalanine	$C_9H_{11}NO_2$	165.07	165.19	1.542	12.230.232.258	99.9
trans-3-Indoleacrylic acid	$C_{11}H_9NO_2$	187.06	187.19	2.355	8.081.509.385	93.4
Cyclo(phenylalanyl-prolyl)	$C_{14}H_{16}N_2O_2$	244.12	454.60	6.168	6.573.460.987	98.3
Prolylleucine	$C_{11}H_{20}N_2O_3$	228.14	362.40	1.98	5.415.498.381	99.7
3-(propan-2-yl)-octahydropyrrolo[1,2-a]pyrazine-1,4-dione	$C_{10}H_{16}N_2O_2$	196.12	196.25	3.945	3.611.552.883	97
L-Norleucine	$C_6H_{13}NO_2$	131.09	131.17	1.248	3.395.525.145	99.4
3-[(4-hydroxyphenyl) methyl]-octahydropyrrolo[1,2-a]pyrazine-1,4-dione	$C_{14}H_{16}N_2O_3$	260.11	260.29	3.968	3.393.892.248	98.7
Bis(2-ethylhexyl) phthalate	$C_{24}H_{38}O_4$	390.27	390.6	17.63	2.141.462.583	99.9
Erucamide	$C_{22}H_{43}NO$	337.33	337.6	17.002	1.545.633.257	97.3
L-(-)-Methionine	$C_5H_{11}NO_2S$	149.05	149.21	0.935	1.071.222.936	98.9
D-(+)-Pipecolinic acid	$C_6H_{11}NO_2$	129.079	129.16	0.896	1.024.001.019	99.5
L-Histidine	$C_6H_9N_3O_2$	155.06	155.15	0.971	981.862.558.3	99.9
Valine	$C_5H_{11}NO_2$	117.07	117.15	1.041	853.583.654.2	99.7
D-(+)-Proline	$C_5H_9NO_2$	115.06	115.13	0.954	703.785.573.8	99.7

BP1-P Extracts						
Name of compound	**Formula**	**Molecular weight**		**RT [min]**	**Area (Max.)**	**mzCloud best match**
		Calculation	**Reference**			
7-(tert-butyl)-4-imino-1,2,3,4,5,6-hexahydropyrido[3,4-d]pyridazine-1,5-dione	$C_{11}H_{14}N_4O_2$	234.11	276.4	1.226	688.315.007.9	85.9
3-(1-hydroxyethyl)-2,3,6,7,8,8a-hexahydropyrrolo[1,2-a]pyrazine-1,4-dione	$C_9H_{14}N_2O_3$	198.10	198.22	1.466	321.520.801	91.4
Indole	C_8H_7N	117.05	117.15	2.355	275.082.770.3	92.2
N-Benzylformamide	C_8H_9NO	135.06	135.16	4.183	274.973.286.1	97.6
4-Indolecarbaldehyd	C_9H_7NO	145.05	145.16	2.369	236.678.245.9	98.7
L-Pyroglutamic	$C_5H_7NO_3$	129.04	129.11	1.19	222.575.598.4	89.1

(A)

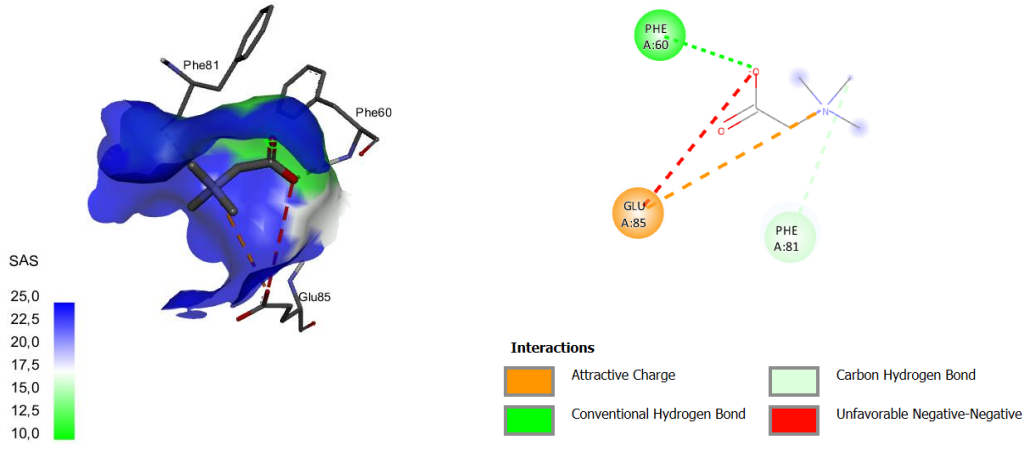

(B)

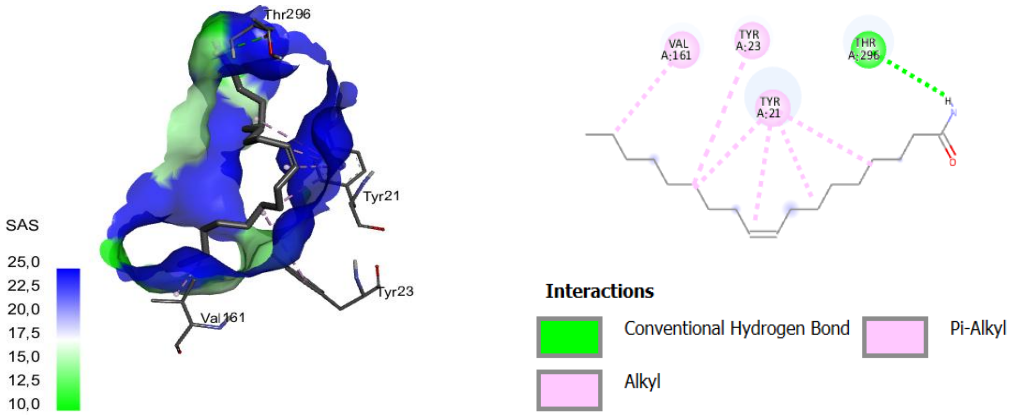

(C)

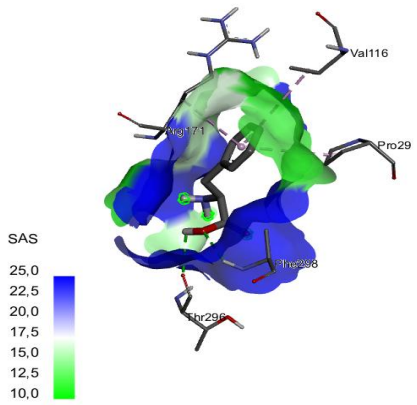
Val116
Pro29
Thr298
Thr296
SAS
25,0
22,5
20,0
17,5
15,0
12,5
10,0

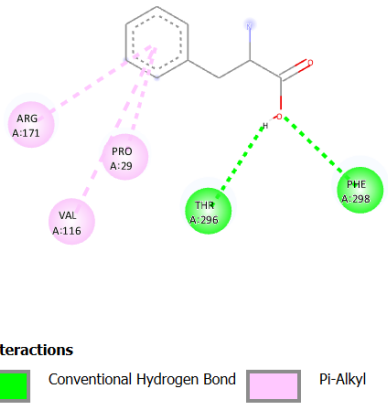
ARG A:171
PRO A:29
VAL A:116
THR A:296
PHE A:298
Interactions
Conventional Hydrogen Bond
Pi-Alkyl

(D)

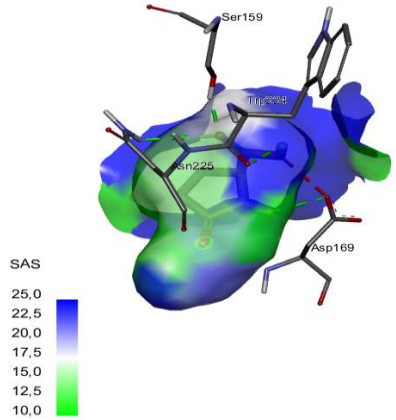
Ser159
Trp224
Asn225
Asp169
SAS
25,0
22,5
20,0
17,5
15,0
12,5
10,0

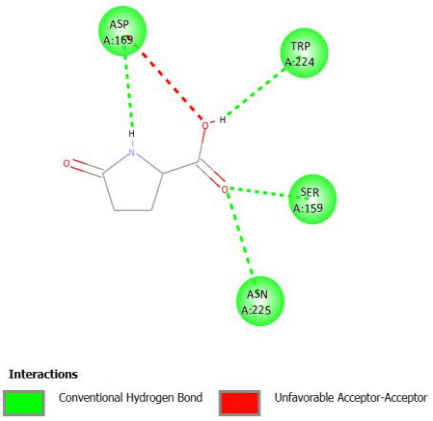
ASP A:169
TRP A:224
SER A:159
ASN A:225
Interactions
Conventional Hydrogen Bond
Unfavorable Acceptor-Acceptor

(E)

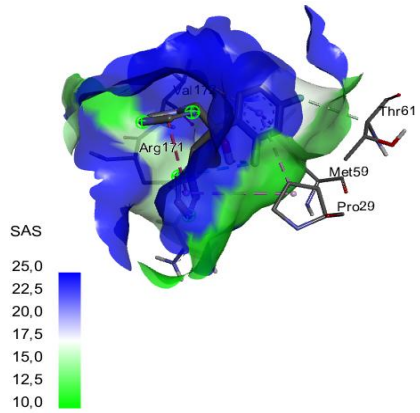
Arg171
Thr61
Met59
Pro29
SAS
25,0
22,5
20,0
17,5
15,0
12,5
10,0

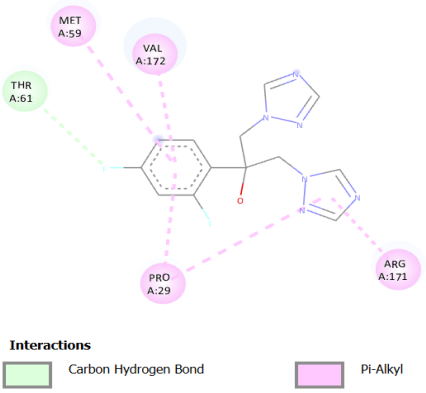
MET A:59
VAL A:172
THR A:61
PRO A:29
ARG A:171
Interactions
Carbon Hydrogen Bond
Pi-Alkyl

(F)

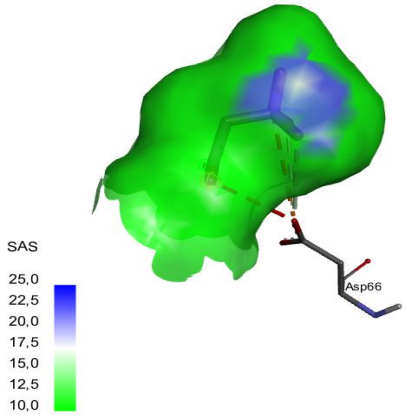
Asp66
SAS
25,0
22,5
20,0
17,5
15,0
12,5
10,0

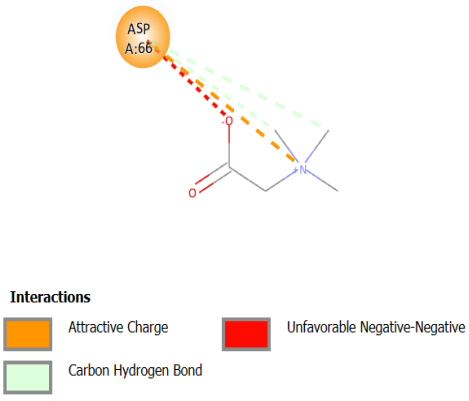
ASP A:66
Interactions
Attractive Charge
Unfavorable Negative-Negative
Carbon Hydrogen Bond

(G)

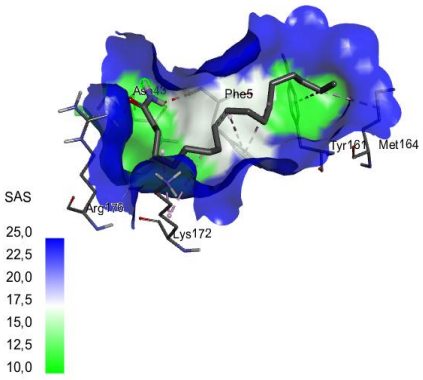
Phe5
Tyr161
Met164
Lys172
SAS
25,0
22,5
20,0
17,5
15,0
12,5
10,0

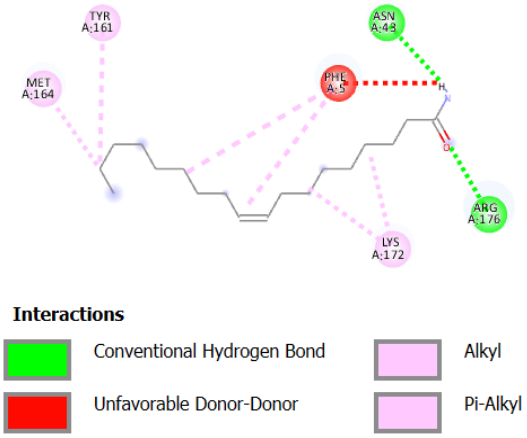
TYR A:161
ASN A:48
MET A:164
PHE A:5
ARG A:176
LYS A:172
Interactions
Conventional Hydrogen Bond
Alkyl
Unfavorable Donor-Donor
Pi-Alkyl

(H)

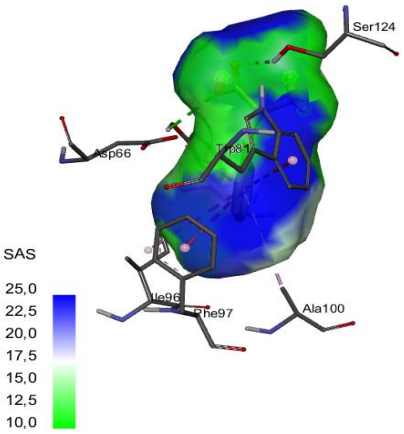
Ser124
Asp66
Trp81
Ile96
Phe97
Ala100
SAS
25,0
22,5
20,0
17,5
15,0
12,5
10,0

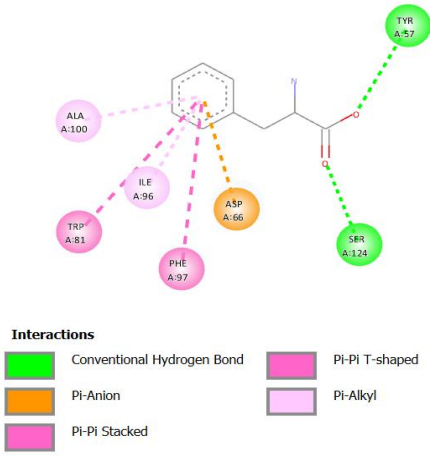
TYR A:57
ALA A:100
ILE A:96
ASP A:66
TRP A:81
PHE A:97
SER A:124
Interactions
Conventional Hydrogen Bond
Pi-Pi T-shaped
Pi-Anion
Pi-Alkyl
Pi-Pi Stacked

(I)

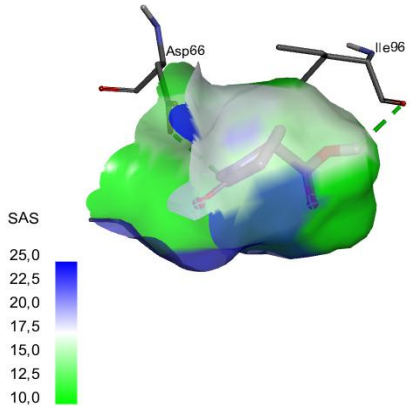
Asp66
Ile96
SAS
25,0
22,5
20,0
17,5
15,0
12,5
10,0

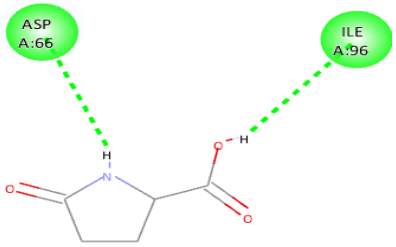
ASP A:66
ILE A:96
Interactions
Conventional Hydrogen Bond

(J)

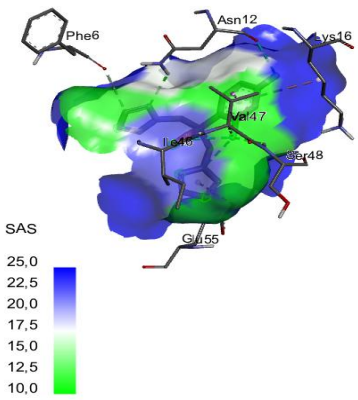
Phe6
Asn12
Lys16
Val47
Ile46
Ser48
Glu55
SAS
25,0
22,5
20,0
17,5
15,0
12,5
10,0

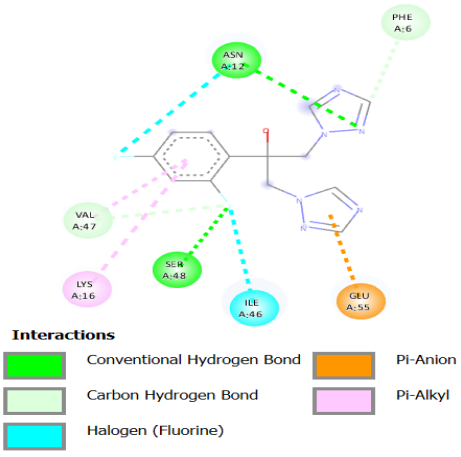
PHE A:6
ASN A:12
VAL A:47
SER A:48
LYS A:16
ILE A:46
GLU A:55
Interactions
Conventional Hydrogen Bond
Pi-Anion
Carbon Hydrogen Bond
Pi-Alkyl
Halogen (Fluorine)

(K)

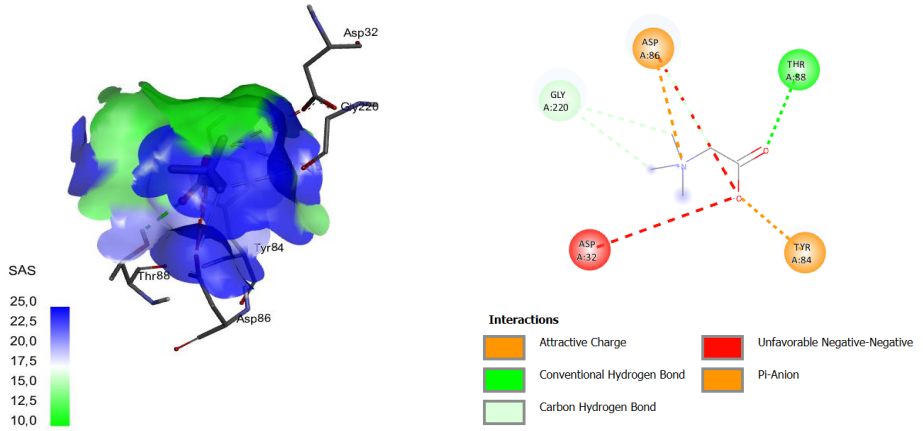
Asp32
Gly220
Tyr84
Thr88
Asp86
SAS
25,0
22,5
20,0
17,5
15,0
12,5
10,0
ASP A:86
THR A:88
GLY A:220
ASP A:32
TYR A:84
Interactions
Attractive Charge
Unfavorable Negative-Negative
Conventional Hydrogen Bond
Pi-Anion
Carbon Hydrogen Bond

(L)

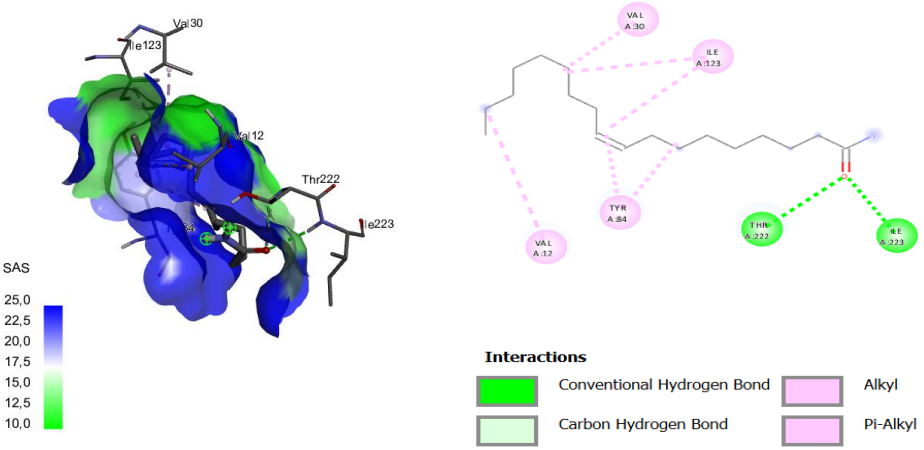
Val30
Ile123
Val12
Thr222
Ile223
SAS
25,0
22,5
20,0
17,5
15,0
12,5
10,0
VAL A:30
ILE A:123
TYR A:84
VAL A:12
Interactions
Conventional Hydrogen Bond
Alkyl
Carbon Hydrogen Bond
Pi-Alkyl

(M)

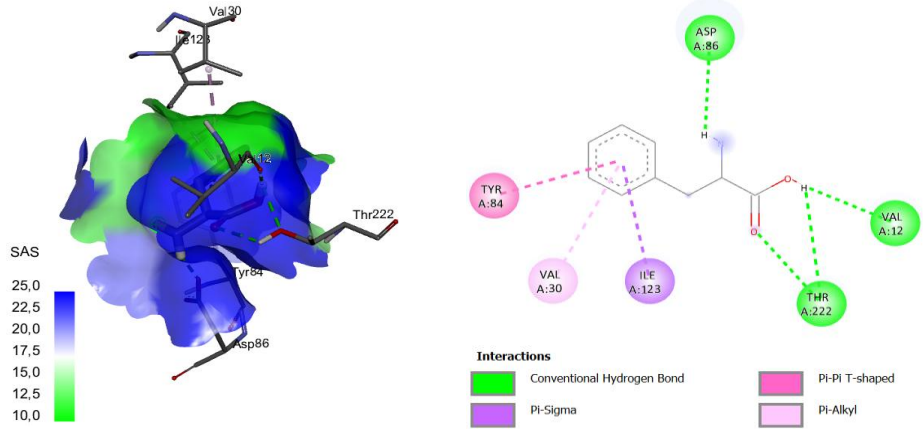
Val30
Ile123
Val12
Thr222
Tyr84
Asp86
SAS
25,0
22,5
20,0
17,5
15,0
12,5
10,0
ASP A:86
TYR A:84
VAL A:12
VAL A:30
ILE A:123
THR A:222
Interactions
Conventional Hydrogen Bond
Pi-Pi T-shaped
Pi-Sigma
Pi-Alkyl

(N)

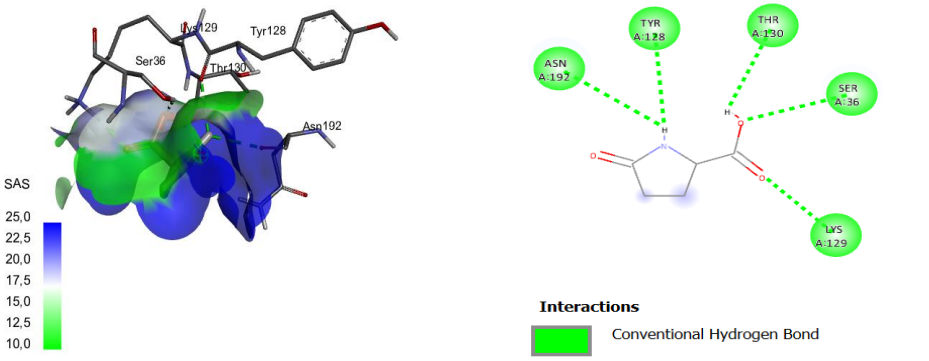
Lys129
Tyr128
Ser36
Thr130
Asp192
SAS
25,0
22,5
20,0
17,5
15,0
12,5
10,0
TYR A:128
THR A:130
ASN A:192
SER A:36
LYS A:129
Interactions
Conventional Hydrogen Bond

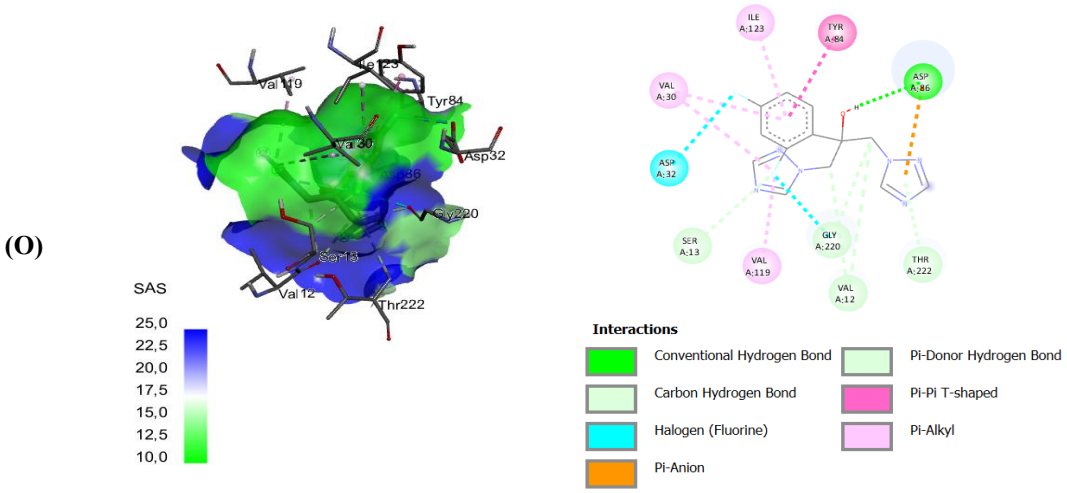

Figure 1(S) 3D and 2D visualization of binding between betaine (A), (F), (K), oleamide (B), (G), (L), l-phenylalanine (C), (H), (M), l-pyroglutamic (D), (I), (N) and fluconazole (E), (J), (O) compounds with ALS3 (1), HWP1 (2) and SAP3 (3) protein, respective interacting amino acid residues.